
Deterministic Inference of Neural Stochastic Differential Equations

Andreas Look¹, Chen Qiu¹, Maja Rudolph¹, Jan Peters², Melih Kandemir¹

¹**Bosch Center for Artificial Intelligence**
Renningen, Germany
`{firstname.lastname}@de.bosch.com`

²**Intelligent Autonomous Systems**
TU Darmstadt, Germany
`peters@ias.tu-darmstadt.de`

Abstract

Model noise is known to have detrimental effects on neural networks, such as training instability and predictive distributions with non-calibrated uncertainty properties. These factors set bottlenecks on the expressive potential of Neural Stochastic Differential Equations (NSDEs), a model family that employs neural nets on both drift and diffusion functions. We introduce a novel algorithm that solves a generic NSDE using only deterministic approximation methods. Given a discretization, we estimate the marginal distribution of the Itô process implied by the NSDE using a recursive scheme to propagate deterministic approximations of the statistical moments across time steps. The proposed algorithm comes with theoretical guarantees on numerical stability and convergence to the true solution, enabling its computational use for robust, accurate, and efficient prediction of long sequences. We observe our novel algorithm to behave interpretably on synthetic setups and to improve the state of the art on two challenging real-world tasks.

1 Introduction

Ordinary Differential Equations (ODE) are the standard tools to model dynamical environments from first principles. Neural networks have long been viewed as black-boxes and have been used to model either non-linear state transitions across discrete time steps [Hochreiter and Schmidhuber, 1997, Cho et al., 2014] or as deep feed-forward sequence models, that convolve across time with or without autoregressive feedback [Bai et al., 2019, Yu and Koltun, 2016]. Alternative approaches to neural networks for state space modeling used Gaussian Processes (GP) [Frigola et al., 2013, Doerr et al., 2018] or directly targeted to learn a set of nonlinearities [Brunton et al., 2016]. While enabling a breakthrough in domains with discrete state evolution [Cho et al., 2014, Bahdanau et al., 2014], their applicability to continuous dynamics remained as an active field of research. Seminal work such as Neural ODEs (NODEs) [Chen et al., 2018] has addressed this question by proposing a third option: modeling an ODE as a neural network and backpropagating the error on discrete observations. This approach ignited a line of follow up work, which focused on exact gradient estimation [Gholami et al., 2019], time evolving parameters [Zhang et al., 2019], and sparse systems [Ayed et al., 2019].

Many dynamical environments exhibit a stochastic nature due to uncaptured factors. Hence, recent work has considered extending NODEs to stochastic dynamics by employing neural nets for both drift and diffusion terms [Look and Kandemir, 2019, Tzen and Raginsky, 2019], which is referred to as *Neural Stochastic Differential Equations (NSDEs)*. The main body of prior work uses the Euler-Maruyama (EM) discretization, while the Milstein discretization [Li et al., 2020] enables a higher convergence order in the strong sense. The common characteristic of these methods is the strong dependency on drawing samples. Similar lines of work spanned placing a GP on the drift

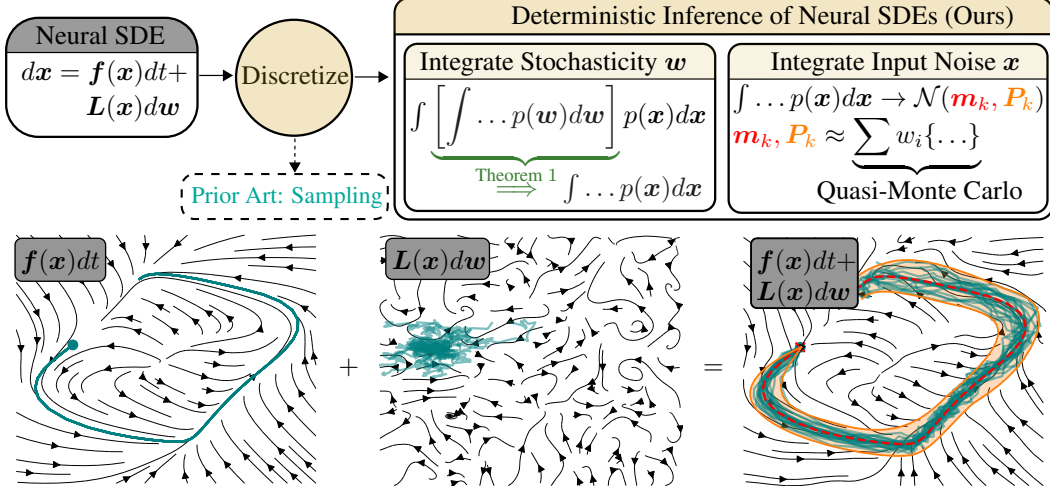


Figure 1: Our algorithm infers an Euler-Maruyama discretized neural SDE by recursive and deterministic moment matching across time steps. The moment matching rule necessitates integration of stochasticity and input noise. We take the former integral analytically by our novel Theorem 1 and use a quasi-Monte Carlo method for the latter. The resultant algorithm is provably stable (Theorem 2) and consistent with the true solution (Theorem 3).

[Heinonen et al., 2018], incorporating second-order dynamics [Yildiz et al., 2019], and modeling a Stochastic Differential Equation (SDE) with a GP [Hegde et al., 2019].

A NSDE with drift and diffusion neural networks does not have a closed-form solution due to: i) the implied SDE not being analytically solvable, and ii) the density of the stochastic process being available only via the Fokker-Planck-Kolmogorov (FPK) equation, which can not be solved without high cost or error. Earlier work approximates (i) by linear dynamics minimizing variational free energy [Archambeau et al., 2007, Duncker et al., 2019] and (ii) by approximations build on learning-based numerics [Raissi and Karniadakis, 2018, Sirignano and Spiliopoulos, 2018, Raissi, 2018]. Current NSDE models suffer from two pain points. First, learning dynamics with neural networks may result in an unstable learning procedure, which can happen even for deterministic model families [Zhang et al., 2018, Jose et al., 2018, Kusupati et al., 2018]. Noise injected as Brownian motion and inaccurate discretization add multiple factors to induce further instabilities. Additionally, NSDE models build on sampling, which introduces a significant computational overhead when a downstream application requires quantification of the uncertainty of predicted trajectories.

This paper presents the first deterministic inference method tailored for generic NSDEs that maintain the key strength of NSDEs, i.e. nonlinearity, while assuring stable training, consistency with the true solution, and efficient access to prediction uncertainties. Our technical contributions are:

- We introduce a novel algorithm, that deterministically approximates the first two moments of the marginal distribution of the Itô process of an NSDE at a time step, given the moments of the previous time step (see Fig. 1).
- We propose a novel moment-matching rule consisting of two deterministic integration steps. The first is achieved by applying our novel Theorem 1, that analytically integrates out stochasticity. The second step uses quasi-Monte Carlo for the first time in the context of NSDEs in order to integrate out the input noise.
- Applying the two-step moment matching rule repetitively towards time steps in the forward direction, we arrive at a recursive algorithm, that both solves the NSDE and allows end-to-end training of its free parameters (i.e. drift and diffusion network parameters).
- Our method comes with plausible theoretical guarantees: numerical stability (Theorem 2) and convergence to the true solution with shrinking step size (Theorem 3).

We demonstrate superior performance and stability of our approach compared to different alternatives.

2 Neural Stochastic Differential Equations

SDEs. A Stochastic Differential Equation (SDE) can be expressed in the following generic form:

$$d\mathbf{x} = \mathbf{f}_\theta(\mathbf{x}, t)dt + \mathbf{L}_\phi(\mathbf{x}, t)d\mathbf{w}, \quad (1)$$

with the potentially nonlinear vector-valued drift function $\mathbf{f}_\theta(\mathbf{x}, t) \in \mathbb{R}^D$, which models the deterministic dynamics, and another potentially nonlinear matrix-valued diffusion function $\mathbf{L}_\phi(\mathbf{x}, t) \in \mathbb{R}^{D \times S}$, which models the stochasticity of the system. Further, dt represents the time increment and $\mathbf{w}(t) \in \mathbb{R}^S$ is chosen to be a Wiener process. The SDE follows a fractal structure, i.e. keeping its wiggly structure even at small time intervals. Consequently, the majority of the SDEs do not have a closed-form solution. Even though the Fokker-Planck-Kolmogorov (FPK) equation characterizes the time evolution of the marginal density of the SDE $p(\mathbf{x}, t)$, the resultant Partial Differential Equation (PDE) is either not analytically tractable. There exist attempts for end-to-end differentiable numerical approximations to the FPK of SDEs, such as [Chen and Duvenaud \[2019\]](#). However using this approach, it is not possible to estimate the marginal density. Further there is no direct coupling between the SDE and the learned $p(\mathbf{x})$, instead $p(\mathbf{x})$ is modeled as a static distribution.

Discretization of SDEs. Numerical solutions to SDEs typically build on discretization of the time domain and approximation of the time step transitions. Due to its computational efficiency and widespread applicability, we adopt the Euler-Maruyama discretization method

$$\tilde{\mathbf{x}}_{k+1}^{(\theta, \phi)} = \mathbf{x}_k + \mathbf{f}_\theta(\mathbf{x}_k, t_k)\Delta t + \mathbf{L}_\phi(\mathbf{x}_k, t_k)\Delta \mathbf{w}_k, \quad (2)$$

where $\Delta \mathbf{w}_k \sim \mathcal{N}(0, \Delta t)$. This method enables sampling-based approximation of moments [[Hegde et al., 2019](#)] and also calculation of these in closed form, as will be detailed in the later chapters. Higher order approximations can be obtained by applying the Itô-Taylor expansion [[Kloeden and Platen, 2013](#)] or stochastic Runge-Kutta methods [[Särkkä and Solin, 2019](#)]. On the downside, higher order approximations demand high computation cost due to the noise term \mathbf{w} . The Milstein discretization [[Li et al., 2020](#)] has the same weak convergence order [[Särkkä and Solin, 2019](#)] as EM discretization. Therefore, EM should be preferred when the statistical properties are of interest.

NSDEs and their inference problems. The term *Neural Stochastic Differential Equation (NSDE)* refers to the case when $\mathbf{f}_\theta(\cdot, \cdot)$ and potentially also $\mathbf{L}_\phi(\cdot, \cdot)$ are neural networks with synaptic weights θ and ϕ , respectively. Even for modestly wide and deep architectures, the resultant NSDE may have thousands of free parameters, making much of the existing parameter identification approaches inapplicable [[Ryder et al., 2018](#), [Abbatì et al., 2019](#)].

3 Deterministic Inference of NSDEs (DI-NSDE)

The first step in developing a sample-free NSDE inference algorithm is to approximate the distribution of a stochastic process. In order to benefit from the tractability properties and general appropriateness to data, we choose $p(\mathbf{x}, t) \approx \mathcal{N}(\mathbf{x}|\mathbf{m}(t), \mathbf{P}(t))$, which amounts to a Gaussian Process (GP) approximation [[Archambeau et al., 2007](#)] with time-evolving mean and covariance. Given a K -step discretization $\{t_k \in [0, T] | k = 1, \dots, K\}$ of an interval $[0, T]$ for arbitrary $T \in \mathbb{R}^+$ and $K \in \mathbb{N}$, the attached time evolution of the distribution of the process variables $\mathbf{x}_1, \dots, \mathbf{x}_K$ follows the series $p(\mathbf{x}_1, t_1), p(\mathbf{x}_2, t_2), \dots, p(\mathbf{x}_K, t_K)$. The elements of this series can be approximated by recursive moment matching in forward index direction. For instance, the marginal distribution of variable \mathbf{x}_{k+1} at time point t_{k+1} can be assumed to follow a Gaussian density

$$p_{\theta, \phi}(\mathbf{x}_{k+1}, t_{k+1}; p_{\theta, \phi}(\mathbf{x}_k, t_k)) \approx \mathcal{N}(\mathbf{x}_{k+1} | \mathbf{m}_{k+1}, \mathbf{P}_{k+1}), \quad (3)$$

with moments computed from the *already matched* moments of the distribution at the preceding time point $p_{\theta, \phi}(\mathbf{x}_k, t_k)$. The recursive moment matching rules are as below [[Särkkä, 2013](#)]:

$$\mathbf{m}_{k+1} \triangleq \int \int_{\mathbb{R}^{D \times S}} \tilde{\mathbf{x}}_{k+1}^{(\theta, \phi)} \underbrace{p_{\theta, \phi}(\mathbf{x}_k, t_k)}_{\approx \mathcal{N}(\mathbf{x}_k | \mathbf{m}_k, \mathbf{P}_k)} p(\mathbf{w}_k) d\mathbf{w}_k d\mathbf{x}_k, \quad (4)$$

$$\mathbf{P}_{k+1} \triangleq \int \int_{\mathbb{R}^{D \times S}} (\tilde{\mathbf{x}}_{k+1}^{(\theta, \phi)} - \mathbf{m}_{k+1})(\tilde{\mathbf{x}}_{k+1}^{(\theta, \phi)} - \mathbf{m}_{k+1})^T \underbrace{p_{\theta, \phi}(\mathbf{x}_k, t_k)}_{\approx \mathcal{N}(\mathbf{x}_k | \mathbf{m}_k, \mathbf{P}_k)} p(\mathbf{w}_k) d\mathbf{w}_k d\mathbf{x}_k, \quad (5)$$

where the dependency of $p_{\theta,\phi}(\mathbf{x}_k, t_k)$ on the previous time step is established by approximating it with $\mathcal{N}(\mathbf{x}_k | \mathbf{m}_k, \mathbf{P}_k)$. Note the nuance in Eq. 3 that

$$p_{\theta,\phi}(\mathbf{x}_{k+1}, t_{k+1}; p_{\theta,\phi}(\mathbf{x}_k, t_k)) \neq p_{\theta,\phi}(\mathbf{x}_{k+1}, t_{k+1} | \mathbf{x}_k). \quad (6)$$

While the l.h.s. takes the entire functional form of density $p_{\theta,\phi}(\mathbf{x}_k, t_k)$, the r.h.s. uses only a sample from it. It is the recurrence relation on the l.h.s. that ties the densities of the individual time points together. The marginal density $p_{\theta,\phi}(\mathbf{x}_{k+1}, t_{k+1})$ is a function of the neural net parameters (θ, ϕ) via $\tilde{\mathbf{x}}_{k+1}^{(\theta,\phi)}$. This recursive density build-up method can be used to model a sequence of arbitrary length with observations at arbitrary and irregular time points. Assume a data set of N time series $\mathcal{D} = \{\widehat{\mathbf{X}}_1, \dots, \widehat{\mathbf{X}}_N\}$, where $\widehat{\mathbf{X}}_n = \{(\widehat{\mathbf{x}}_1^{(n)}, t_1^{(n)}), \dots, (\widehat{\mathbf{x}}_K^{(n)}, t_K^{(n)})\}$ is the n -th sequence in the data set with observation length K . The parameters of the resultant system can then be identified by maximum likelihood estimation (MLE):

$$\underset{\theta, \phi}{\text{maximize}} \underbrace{\sum_{n=1}^N \sum_{k=1}^{K_n-1} \log p_{\theta,\phi}(\widehat{\mathbf{x}}_{k+1}^{(n)}, t_{k+1}^{(n)}; p_{\theta,\phi}(\widehat{\mathbf{x}}_k^{(n)}, t_k^{(n)}))}_{\substack{\text{coupled via recurrence} \\ \text{independent across sequences}}} \quad (7)$$

As a contribution to the prior art, we apply the assumed Gaussian density framework to neural SDE inference in a deterministic and end-to-end differentiable manner following the steps below:

- i) a novel deterministic approximation to the nested integrals in Eqs. 4-5 by two-step marginalization detailed in Sections 3.1 and 3.2,
- ii) recursive building of the computational graph to take the sum $\sum_{k=1}^{K_n-1}$,
- iii) efficient parameter update by minibatching around $\sum_{n=1}^N$.

3.1 Marginalizing out the stochasticity by analytical solution

One of our key contributions is the theorem below, which provides a recipe to calculate the moments of the marginal density at an arbitrary time point of discretization t_k , in a way that marginalizes out the Wiener process noise in closed form.

Theorem 1 (marginalizing stochasticity). *If $\tilde{\mathbf{x}}_{k+1}^{(\theta,\phi)}$ follows the Euler-Maruyama discretization, the moment update rules defined in Eqs. 4 and 5 satisfy the below analytical form with integrated out stochastic noise \mathbf{w}_k :*

$$\mathbf{m}_{k+1} = \int_{\mathbb{R}^D} \tilde{\mathbf{x}}_{k+1}^{(\theta,\phi)} \mathcal{N}(\mathbf{x}_k | \mathbf{m}_k, \mathbf{P}_k) d\mathbf{x}_k, \quad (8)$$

$$\mathbf{P}_{k+1} = \int_{\mathbb{R}^D} \left[(\tilde{\mathbf{x}}_{k+1}^{(\theta,\phi)} - \mathbf{m}_{k+1})(\tilde{\mathbf{x}}_{k+1}^{(\theta,\phi)} - \mathbf{m}_{k+1})^T + \mathbf{L}_\phi \mathbf{L}_\phi^T(\mathbf{x}_k, t_k) \Delta t \right] \mathcal{N}(\mathbf{x}_k | \mathbf{m}_k, \mathbf{P}_k) d\mathbf{x}_k, \quad (9)$$

where $\tilde{\mathbf{x}}_{k+1}^{(\theta,\phi)} \triangleq \mathbf{x}_k + \mathbf{f}_\theta(\mathbf{x}_k, t_k) \Delta t$ and Δt is a time step that does not depend on $\Delta \mathbf{w}_k$.

Proof Sketch. First, apply EM discretization to both integrals. Use the identity $\mathbb{E}[\Delta \mathbf{w} \Delta t] = \mathbb{E}[\Delta \mathbf{w}] \mathbb{E}[\Delta t] = 0$ to marginalize out the process noise as $\mathbb{E}[\Delta \mathbf{w}] = 0$. Evaluate off-diagonal covariance entries separately in order to estimate $\mathbb{E}[\Delta \mathbf{w}^2]$. See Appendix A for further details.

3.2 Marginalizing out the input uncertainty by quasi-Monte Carlo integration

As the final step towards attaining a fully deterministic inference algorithm, we need to take the integrals with respect to \mathbf{x}_k in Eqs. 8 and 9. We adopt a quasi-Monte Carlo (QMC) algorithm to approximate these integrals. As both are with respect to normal distributions, we choose the Gaussian cubature algorithm, which approximates the expectation of an arbitrary smooth function $g(\mathbf{x}_k, t_k)$ with respect to a normal distribution $\mathcal{N}(\mathbf{x}_k | \mathbf{m}_k, \mathbf{P}_k)$ as

$$\int g(\mathbf{x}_k, t_k) \mathcal{N}(\mathbf{x}_k | \mathbf{m}_k, \mathbf{P}_k) d\mathbf{x}_k \approx \sum_{i=1}^C w_i g(\mathbf{m}_k + \sqrt{\mathbf{P}_k} \zeta_i, t_k), \quad (10)$$

where $\sqrt{\mathbf{P}_k} \sqrt{\mathbf{P}_k^T} = \mathbf{P}_k$. The coefficients w_i and ζ_i are predetermined by a heuristic that aims to spread the particles around the support of the distribution in a maximally information preserving way. We approximate the integrals in Eqs. 8 and 9 simply by choosing $g(\mathbf{x}_k, t_k) \triangleq \hat{\mathbf{x}}_{k+1}^{(\theta, \phi)}$ for calculation of \mathbf{m}_k and $g(\mathbf{x}_k, t_k) \triangleq (\hat{\mathbf{x}}_{k+1}^{(\theta, \phi)} - \mathbf{m}_{k+1})(\hat{\mathbf{x}}_{k+1}^{(\theta, \phi)} - \mathbf{m}_{k+1})^T + \mathbf{L}_\phi \mathbf{L}_\phi^T(\mathbf{x}_k, t_k) \Delta t$ for \mathbf{P}_k .

There exist multiple heuristics for choosing w_i and ζ_i . We adopt the unscented transform (UT) [Stenger and Mcnamee, 1967], which can be formulated as a sum of $2D + 1$ elements for a D -dimensional input space as following [Wan and Merwe, 2000]:

$$w_i = \begin{cases} \frac{\lambda}{D+\kappa} & , i = 0, \\ \frac{1}{2(D+\kappa)} & , i = 1, \dots, 2D, \end{cases} \quad \zeta_i = \begin{cases} 0 & , i = 0, \\ \sqrt{\lambda + D} \mathbf{e}_i & , i = 1, \dots, D, \\ -\sqrt{\lambda + D} \mathbf{e}_{i-D} & , i = D + 1, \dots, 2D. \end{cases} \quad (11)$$

Above, λ and κ are predetermined hyperparameters controlling the spread of the approximation points, common choice choices are $\lambda = 0$ and $\kappa = 0$. Setting these parameters to alternative values made ignorable change in our experiments. Vectors \mathbf{e}_i can be chosen arbitrarily as long as they form an orthonormal basis for the input space. We adopt the unit vectors, e.g. $\mathbf{e}_2 = [0, 1, \dots, 0]$. UT is a third order cubature method, which uses three approximation points per dimension. Higher order cubature approximations can be derived at the expense of more function evaluations, e.g. 5th order approximation needs $\mathcal{O}(D^2)$ evaluations and 7th order $\mathcal{O}(D^3)$. See Appendix H for a detailed comparison to layerwise moment matching [Wang et al., 2008].

3.3 The proposed algorithm and its theoretical properties

Plugging in the outcome of Theorem 1 and the aforementioned QMC method into the inference problem in Eq. 7, we attain a fully deterministic solution detailed in Algorithm 1. Below, the means and covariances of the marginals are denoted as $\mathbf{m}_{1:K}$ and $\mathbf{P}_{1:K}$, respectively. The moments of the initial step are \mathbf{m}_1 and \mathbf{P}_1 . One may use $\mathbf{P}_1 \approx \mathbf{I}\epsilon$ and $\mathbf{m}_1 = \hat{\mathbf{x}}_k$ for conditioning on the observed state $\hat{\mathbf{x}}_k$ (Gaussian approximation to Dirac distribution), with ϵ being a small number, which we choose as 10^{-4} . Note that mean at each time step can be estimated either by linearization around \mathbf{m}_k or by applying QMC. Estimating \mathbf{m}_{k+1} by linearization is our default choice, since i) both methods perform approximately equal (see Sec. 5) and ii) linearization is faster. An efficient and differentiable calculation scheme of $\mathcal{N}(\mathbf{x}_k | \mathbf{m}_k, \mathbf{P}_k)$ is described in Appendix F. We also provide a PyTorch implementation of our method in Appendix L.

Algorithm 1 NSDE Training with our method DI-NSDE

```

Inputs:  $f_\theta, \mathbf{L}_\phi, \mathcal{D}$ 
Outputs: Optimized  $\theta, \phi$ 
def Main()
  while not converged do
     $\{(\hat{\mathbf{x}}_1^{(n)}, t_1^{(n)}), \dots, (\hat{\mathbf{x}}_{K_n}^{(n)}, t_{K_n}^{(n)})\} \sim \mathcal{D}$  ▷ Sample from  $\mathcal{D}$ 
     $\mathbf{m}_1 = \hat{\mathbf{x}}_1^{(n)}, \mathbf{P}_1 = \mathbf{I}\epsilon$  ▷ Gaussian Approximation to Dirac
     $\mathbf{m}_{1:K}, \mathbf{P}_{1:K} = \text{DI\_NSDE}(\mathbf{m}_1, \mathbf{P}_1, t_{1:K}^{(n)})$ 
     $\theta, \phi = \underset{\theta, \phi}{\text{maximize}} \sum_{k=2}^K \log \mathcal{N}(\hat{\mathbf{x}}_k^{(n)} | \mathbf{m}_k, \mathbf{P}_k)$  ▷ MLE of Parameters Eq. 7
  return  $\theta, \phi$ 
def DI_NSDE( $\mathbf{m}_1, \mathbf{P}_1, t_{1:K}$ ) ▷ Theorem 1
  for  $k \leftarrow 1 : K - 1$  do
     $\mathbf{m}_{k+1} = \text{MeanInt}(\mathbf{m}_k, t_k)$  \\or  $\text{UTSolve}(\mathbf{m}_k, \mathbf{P}_k, t_k, \text{MeanInt}(\cdot, \cdot))$  ▷ Linearize or QMC
     $\mathbf{P}_{k+1} = \text{UTSolve}(\mathbf{m}_k, \mathbf{P}_k, t_k, \text{CovInt}(\cdot, \cdot, \mathbf{m}_{k+1}))$  ▷ QMC
  return  $\mathbf{m}_{1:K}, \mathbf{P}_{1:K}$ 
def MeanInt( $\mathbf{x}, t$ ) ▷ Mean integral Eq. 8
  return  $\mathbf{x} + f_\theta(\mathbf{x}, t) \Delta t$ 
def CovInt( $\mathbf{x}, t, \mathbf{m}$ ) ▷ Covariance integral Eq. 9
   $\mathbf{g} = \mathbf{x} + f_\theta(\mathbf{x}, t) \Delta t - \mathbf{m}$ 
   $\mathbf{g} \mathbf{g}^T(\mathbf{x}, t) + \mathbf{L}_\phi \mathbf{L}_\phi^T(\mathbf{x}, t) \Delta t$ 
def UTSolve( $\mathbf{m}, \mathbf{P}, t, \mathbf{g}$ ) ▷ Unscented Transform Eq. 10 and 11
  Initialize  $\mathbf{v} = 0$ 
   $\mathbf{w}_{0:2D}, \zeta_{0:2D} = \text{SigmaPoints}(D, \lambda, \kappa)$ 
  for  $d \leftarrow 0 : 2D$  do
     $\mathbf{x} = \mathbf{m} + \sqrt{\mathbf{P}} \zeta_d$ 
     $\mathbf{v} += \mathbf{g}(\mathbf{x}, t) w_d$ 
  return  $\mathbf{v}$ 

```

We analyze the theoretical properties of our method from two perspectives: i) numerical stability, and ii) convergence to the true solution. As the main source of numerical failures in recursive moment matching is singular covariance matrices, we first define a stability criterion based on positive semi-definiteness of the covariance matrices and then prove that DI-NSDE satisfies this criterion.

Definition 1 (covariance stability). Let $\tilde{x}_{k+1} \triangleq h(\tilde{x}_k)$ be an update rule used by an SDE inference algorithm at time step t_{k+1} of a K -step discretization $\{t_1, \dots, t_K\}$ of a continuous time interval $[t_1, t_K]$ for an arbitrarily large integer K . Also let $\tilde{p}(\tilde{x}_{k+1}, t_{k+1})$ be the approximate marginal density the algorithm outputs. This SDE inference algorithm is called to be "covariance stable" if $\text{Cov}_{\tilde{p}}(\tilde{x}_{k+1})$ is positive semi-definite (PSD) for all $k \in \{1, \dots, K-1\}$.

Theorem 2 (DI-NSDE is covariance stable). The deterministic SDE inference procedure that uses the moment matching procedure given in Theorem 1 to integrate out w_k and the QMC approximation described in Eq. 10 to integrate out x_k is covariance stable if $\text{Cov}_{\tilde{p}}(\tilde{x}_1)$ is positive semi-definite.

We prove that our method converges to the true solution as the step size shrinks with order 1. Weak convergence of our moment-matching based method appears naturally as a straightforward extension of the plain EM proof [Kloeden and Platen, 2013]. See Appendix B and C for details of both proofs.

Theorem 3 (weak convergence). Let $p(x)$ be a normal distribution and $f_\theta(x)$, $L_\phi(x)$ follow the linear growth and c_2 -Lipschitz condition. The approximate prediction $\mathbf{g}(\tilde{x}_k, t_k)$ obtained at time t_k by the update rules defined in Theorem 1 followed by a quasi-Monte Carlo approximation converges weakly to the true solution $\mathbf{g}(x_k, t_k)$ with order 1 as the number C of quasi-Monte Carlo approximation points $C \rightarrow \infty$

$$\sup_{0 \leq t_k \leq T} \left| \mathbb{E}[\mathbf{g}(x_k, t_k)] - \mathbb{E}[\mathbf{g}(\tilde{x}_k, t_k)] \right| \leq S \Delta t,$$

for any $T > 0$, any smooth function $\mathbf{g}(\cdot)$, and some $S \in \mathbb{R}^+$.

4 Alternative Methods

A straightforward alternative to our method is to fit a deterministic ODE on the mean ($\frac{\partial \mathbf{m}}{\partial t} = \dot{\mathbf{m}}$) and covariance of the marginal density function ($\frac{\partial \mathbf{P}}{\partial t} = \dot{\mathbf{P}}$) and solve via (i) cubature approximation (ODEA_{UT}) or (ii) linearization (ODEA_{Lin.}). See Appendix D for details and derivations.

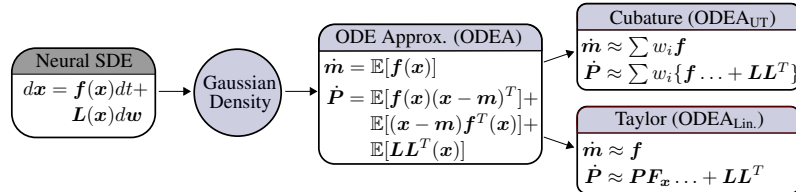


Figure 2: Alternative methods rely on approximating firstly the marginal density as a Gaussian distribution. Mean and covariance evolution are governed by two ODEs, which can be solved via (i) cubature (ODEA_{UT}) or (ii) linearization (ODEA_{Lin.}).

Another alternative approach is obtained by a discretization scheme and estimating mean and covariance by sampling. Using EM discretization together with the sample based scheme, the marginal density is approximated as $p(x_{k+1}|x_k + f_\theta(x_k)\Delta t, L_\phi L_\phi^T(x_k, t_k)\Delta t)$. We refer to this approach as NSDE_{MC} [Look and Kandemir, 2019, Chen and Duvenaud, 2019]. Lastly, it is also possible to use linearization of the update rule after EM discretization, which would give closed-form access to mean and covariance. This approach accumulates model uncertainty rapidly through time, resulting in lower uncertainty calibration scores than our method, as we observed in our preliminary tries. We omit this comparison for brevity. Below we review the properties of each method. Table 1 compares our proposed method DI-NSDE to its variants: (i) NSDE_{MC} (sampling), (ii) ODEA_{UT}, (iii) ODEA_{Lin.}.

Covariance Stability. Our method DI-NSDE comes with stability guarantees (Theorem 2). When using another discretization schemes than Euler-Maruyama, e.g. Itô-Taylor scheme of order 1.5 [Arasaratnam et al., 2010], stability is not guaranteed. When using explicit or adaptive step size solvers [Chen et al., 2018], stability is not ensured for $\text{ODEA}_{\text{UT/Lin.}}$. The solution of $\text{ODEA}_{\text{Lin.}}$ may be stabilized by specialized solvers, development of which is an open research topic. See Appendix E for a discussion about numerical properties regarding both ODEA variants. The sampling-based NSDE_{MC} is covariance stable, since computed covariances is not propagated across multiple time steps.

Complexity. We measure complexity as the number of NSDE evaluations during prediction for one future time step. We assume to use EM discretization for NSDE_{MC} , DI-NSDE and Euler discretization for $\text{ODEA}_{\text{UT/Lin.}}$ for this discussion. The sampling based method NSDE_{MC} depends on the chosen number of particles P , which requires a single NSDE evaluation per particle $\mathcal{O}(P)$. When using DI-NSDE, evaluation of $2D + 1$ cubature points is necessary, hence $\mathcal{O}(D)$. Same applies for ODEA_{UT} . When using $\text{ODEA}_{\text{Lin.}}$ evaluation of the Jacobian with D^2 elements becomes necessary.

Estimator Variance. All closed form approximations rely on deterministic operations only, hence zero estimator variance. By contrast, the sampling based alternative NSDE_{MC} introduces variance on the estimator of the data likelihood, stemming from randomness due to sampling.

5 Experiments

We benchmark DI-NSDE on one standard synthetic setup and two real-world data sets. We refer to our method as $\text{DI-NSDE}_{\text{UT}}$, when using the UT to estimate \mathbf{m}_k , and as $\text{DI-NSDE}_{\text{Lin.}}$, when using linearization. We also present in Appendix G a study analyzing the behaviour of our method on a synthetic multimodal distribution. For $\text{ODEA}_{\text{UT/Lin.}}$, we use a Runge-Kutta solver of 4th order. Due to numerical considerations [Gholami et al., 2019], we backpropagate directly through the computational graph, which is created by the solver, instead of using the adjoint method [Chen et al., 2018]. Hyperparameters have been tuned manually for each method.

Lotka-Volterra. This experiment illustrates the qualitative behavior of DI-NSDE on the stochastic Lotka-Volterra dynamics (see Appendix I for details). We generate 128 paths using Euler-Maruyama discretization with a small step size of $dt = 10^{-5}$ seconds. Afterwards, we coarsen the data set such that 200 equally spaced observations between 0 – 10 seconds remain. First 100 observations are used for training and the remaining 100 observations for testing. Deterministic integration methods (DI-NSDE, ODEA) deliver both more accurate predictions and better calibrated uncertainty scores than NSDE_{MC} training, as shown in Table 2 and Figure 3. DI-NSDE outperforms the alternative methods in both prediction accuracy and the quality of predictive uncertainty calibrations.

Weather Forecast. The United States Historical Climatology Network (USHCN) daily dataset [Menne et al., 2015] contains five climate measurements from approximately 1200 USHCN stations. We adopt the preprocessing (making data partially observed) and evaluation procedure from Brouwer et al. [2019]. In order to evaluate the extrapolation capabilities of our method, we extend the original task from performing three step predictions by additionally performing 300 step predictions. See Appendix J.2 for further details regarding the network architecture. Table 2 reports results for 3 and 300 step predictions. The accuracy of our method is on par with the state-of-the-art GOB [Brouwer et al., 2019] for three-step predictions. However, for long-term predictions DI-NSDE improves the state of the art by a significant margin. We attribute this outcome to the stable training procedure and well-preserved uncertainty quantification capabilities thanks to the deterministic inference scheme. We provide prediction visualizations in Appendix K. The alternative method $\text{ODEA}_{\text{Lin.}}$ did not train due to covariance instability of \mathbf{P}_k . As training progresses, stiffness of the neural SDE can change fast. Reducing the step size Δt in order to tackle stiffness does not stabilize ODEA training.

Table 1: Categorical comparison of the proposed solution DI-NSDE to (i) sampling NSDE_{MC} , and (ii) ODE approximation of mean and covariance $\text{ODEA}_{\text{UT/Lin.}}$. Complexity is measured in number of NSDE evaluations during prediction, where P is the # particles and $\mathbf{x}_k \in \mathbb{R}^D$.

Method	Stability (Def. 1)	Complexity $\mathcal{O}(\cdot)$	Estimator Variance
NSDE_{MC}	✓	$\mathcal{O}(P)$	> 0
ODEA_{UT}	✗	$\mathcal{O}(D)$	0
$\text{ODEA}_{\text{Lin.}}$	✗	$\mathcal{O}(D^2)$	0
DI-NSDE	✓	$\mathcal{O}(D)$	0

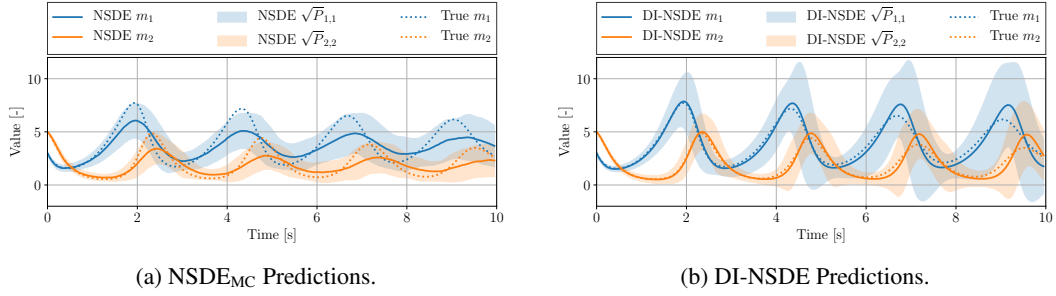


Figure 3: Predictive means and one standard deviation error bars for the sampling-based NSDE_{MC} and our deterministic DI-NSDE for stochastic Lotka-Volterra. In this example, deterministic NSDE integration improves both prediction accuracy and uncertainty calibration.

Table 2: All experiments are extrapolation tasks. We provide for Lotka-Volterra (2dim, 100 step extrapolation) average MSE and standard deviation over 10 runs. Methods used for comparison for CMU-Walking (50dim, 297 step extrapolation) reported best results. We do the same as competitor methods and report additionally the average over 10 runs in brackets. For USHCN (partially observed, 5dim, 3/300 step extrapolation) we report mean and standard deviation for 5-fold-cross-validations. **NaN**: Model training failure in all repetitions due to numerical instability.

Model	Lotka-Volterra		Weather Forecast (3 Step)		Weather Forecast (300 Steps)		CMU
	MSE	NLL	MSE	NLL	MSE	NLL	
Neural-ODE [Chen et al., 2018]	-	-	0.96 \pm 0.11	1.46 \pm 0.10	-	-	21.60
ODE ² VAE-KL [Yildiz et al., 2019]	-	-	-	-	-	-	6.48
Sequential VAE [Krishnan et al., 2017]	-	-	0.83 \pm 0.07	1.37 \pm 0.06	-	-	-
GRU-D [Che et al., 2016]	-	-	0.53 \pm 0.06	0.99 \pm 0.07	-	-	-
T-LSTM [Baytas et al., 2017]	-	-	0.59 \pm 0.11	1.67 \pm 0.50	-	-	-
GRU-ODE-Bayes [Brouwer et al., 2019]	-	-	0.43 \pm 0.07	0.84 \pm 0.11	0.64 \pm 0.06	1.12 \pm 0.12	-
NSDE _{MC}	0.81 \pm 0.06	2.38 \pm 0.08	0.68 \pm 0.19	1.21 \pm 0.10	0.58 \pm 0.06	1.09 \pm 0.04	5.44 (7.26)
ODEA _{UT}	0.82 \pm 0.07	1.68 \pm 0.15	0.39 \pm 0.05	1.04 \pm 0.14	0.59 \pm 0.06	1.03 \pm 0.07	NaN
ODEA _{Lin.}	0.78 \pm 0.09	1.76 \pm 0.22	NaN	NaN	NaN	NaN	5.04 (6.98)
DI-NSDE _{UT} (Ours)	0.76 \pm 0.04	1.65 \pm 0.16	0.37 \pm 0.07	0.95 \pm 0.10	0.57 \pm 0.05	0.96 \pm 0.04	4.75 (6.62)
DI-NSDE _{Lin.} (Ours)	0.77 \pm 0.08	1.79 \pm 0.20	0.35 \pm 0.11	0.91 \pm 0.20	0.55 \pm 0.10	0.91 \pm 0.14	4.77 (6.46)

CMU Motion Capture. We follow Yildiz et al. [2019] for preprocessing and designing the experimental setup using data from the CMU motion capture library. The dataset is constructed accordingly to Gan et al. [2015]. It consists of 23 sequences from Subject 35. The dataset is split into 16 sequences for training, three for validation, and four for test. After preprocessing the dataset consist of 50 dimensions. We use a similar architecture as Yildiz et al. [2019], i.e. an encoder-decoder structure. A sketch of the architecture is given in Appendix J.1. Table 2 summarizes the results for mean predictions. Note that the models used for comparison reported best observed results. For completeness, we report the best outcome, as well as the average obtained over 10 runs. Our method DI-NSDE brings consistent improvement in prediction accuracy. We could not train a neural SDE using ODEA_{UT}, since the predicted covariance P_k was not covariance unstable (not positive semi-definite) as training progressed. In general it is unpredictable whether ODEA training converges.

6 Conclusion and Future Extensions

We introduce a deterministic inference procedure to solve arbitrarily nonlinear neural SDEs, which is computationally stable (Definition 1), consistent with the true solution (Theorem 3) and has better calibrated uncertainty estimates compared to its alternatives. The major limitation of our method is that it cannot model multimodal distributions. A direct extension to our work could be to do moment matching across Gaussian mixtures with ideally variable and learnable number of modes. Also detecting the position or time at which a predicted trajectory can split is of crucial importance for future research. Therefore analysis of exit times [Oksendal, 1992] can serve as a theoretical base. Lastly, one may consider decreasing the number of neural SDE evaluations, by employing Bayesian quadrature [Briol et al., 2015] or particle methods [Liu and Wang, 2016].

References

Gabriele Abbati, Philippe Wenk, Michael Osborne, Andreas Krause, Bernhard Schölkopf, and Stefan Bauer. AReS and MaRS adversarial and MMD-minimizing regression for SDEs. In *ICML*. 2019.

Ienkaran Arasaratnam, Simon Haykin, and Thomas R. Hurd. Cubature kalman filtering for continuous-discrete systems: Theory and simulations. *Trans. Sig. Proc.*, 58, 2010.

Cedric Archambeau, Dan Cornford, Manfred Opper, and John Shawe-Taylor. Gaussian process approximations of stochastic differential equations. *Proceedings of Machine Learning Research*, 1, 2007.

Ibrahim Ayed, Emmanuel de Bézenac, Arthur Pajot, Julien Brajard, and Patrick Gallinari. Learning dynamical systems from partial observations. *ArXiv*, abs/1902.11136, 2019.

Dzmitry Bahdanau, Kyunghyun Cho, and Yoshua Bengio. Neural machine translation by jointly learning to align and translate. In *ICLR*. 2014.

Shaojie Bai, J. Zico Kolter, and Vladlen Koltun. Trellis networks for sequence modeling. In *ICLR*. 2019.

Inci M Baytas, Cao Xiao, Xi Zhang, Fei Wang, Anil K Jain, and Jiayu Zhou. Patient subtyping via time-aware lstm networks. In *KDD*. 2017.

François-Xavier Briol, Chris Oates, Mark Girolami, and Michael A Osborne. Frank-wolfe bayesian quadrature: Probabilistic integration with theoretical guarantees. In *NeurIPS*. 2015.

Edward Brouwer, Jaak Simm, Adam Arany, and Yves Moreau. Gru-ode-bayes: Continuous modeling of sporadically-observed time series. In *NeurIPS*. 2019.

Robert Grover Brown and Patrick Hwang. *Introduction to random signals and applied kalman filtering: with MATLAB exercises and solutions; 3rd ed.* Wiley, 1997.

Steven L. Brunton, Joshua L. Proctor, and J. Nathan Kutz. Discovering governing equations from data by sparse identification of nonlinear dynamical systems. *Proceedings of the National Academy of Sciences*, 113, 2016.

Zhengping Che, Sanjay Purushotham, Kyunghyun Cho, David Sontag, and Yan Liu. Recurrent neural networks for multivariate time series with missing values. *ArXiv*, abs/1606.01865, 2016.

Tian Qi Chen and David K Duvenaud. Neural networks with cheap differential operators. In *NeurIPS*. 2019.

Tian Qi Chen, Yulia Rubanova, Jesse Bettencourt, and David K Duvenaud. Neural ordinary differential equations. In *NeurIPS*. 2018.

Kyunghyun Cho, Bart van Merriënboer, Caglar Gulcehre, Dzmitry Bahdanau, Fethi Bougares, Holger Schwenk, and Yoshua Bengio. Learning phrase representations using RNN encoder–decoder for statistical machine translation. In *EMNLP*. 2014.

Andreas Doerr, Christian Daniel, Martin Schiegg, Nguyen-Tuong Duy, Stefan Schaal, Marc Toussaint, and Trimpe Sebastian. Probabilistic recurrent state-space models. In *ICML*. 2018.

Lea Duncker, Gergo Bohner, Julien Boussard, and Maneesh Sahani. Learning interpretable continuous-time models of latent stochastic dynamical systems. In *ICML*. 2019.

Emilien Dupont, Arnaud Doucet, and Yee Whye Teh. Augmented neural odes. In *NeurIPS*. 2019.

Roger Frigola, Fredrik Lindsten, Thomas B Schön, and Carl Edward Rasmussen. Bayesian inference and learning in gaussian process state-space models with particle mcmc. In *NeurIPS*. 2013.

Zhe Gan, Chunyuan Li, Ricardo Henao, David E Carlson, and Lawrence Carin. Deep temporal sigmoid belief networks for sequence modeling. In *NeurIPS*. 2015.

Amir Gholami, Kurt Keutzer, and George Biros. Anode: Unconditionally accurate memory-efficient gradients for neuralodes. In *IJCAI*. 2019.

Pashupati Hegde, Markus Heinonen, Harri Lähdesmäki, and Samuel Kaski. Deep learning with differential gaussian process flows. In *AISTATS*. 2019.

Markus Heinonen, Cagatay Yildiz, Henrik Mannerström, Jukka Intosalmi, and Harri Lähdesmäki. Learning unknown ODE models with Gaussian processes. In *ICML*. 2018.

Sepp Hochreiter and Jürgen Schmidhuber. Long short-term memory. *Neural computation*, 9, 1997.

Cijo Jose, Moustapha Cisse, and Francois Fleuret. Kronecker recurrent units. In *ICML*. 2018.

P.E. Kloeden and E. Platen. *Numerical Solution of Stochastic Differential Equations*. Springer Berlin Heidelberg, 2013.

Rahul G Krishnan, Uri Shalit, and David Sontag. Structured inference networks for nonlinear state space models. In *AAAI*. 2017.

Aditya Kusupati, Manish Singh, Kush Bhatia, Ashish Kumar, Prateek Jain, and Manik Varma. Fastgrnn: A fast, accurate, stable and tiny kilobyte sized gated recurrent neural network. In *NeurIPS*. 2018.

Xuechen Li, Ting-Kam Leonard Wong, Ricky T. Q. Chen, and David Duvenaud. Scalable gradients for stochastic differential equations. In *AISTATS*. 2020.

Qiang Liu and Dilin Wang. Stein variational gradient descent: A general purpose bayesian inference algorithm. In *NeurIPS*. 2016.

Andreas Look and Melih Kandemir. Differential bayesian neural networks. In *NeurIPS Workshop Bayesian Deep Learning*. 2019.

Hermann Mena and Peter Benner. Numerical solution of differential riccati equations arising in optimal control for parabolic pdes. *Proceedings in Applied Mathematics and Mechanics*, 2007.

MJ Menne, CN Williams Jr, RS Vose, and US Surface Temperature Trends. Long-term monthly climate records from stations across the contiguous united states. 2015.

Bernt Oksendal. *Stochastic Differential Equations: An Introduction with Applications*. Springer, 1992.

Maziar Raissi. Forward-backward stochastic neural networks: Deep learning of high-dimensional partial differential equations. *ArXiv*, abs/1804.07010, 2018.

Maziar Raissi and George Em Karniadakis. Hidden physics models: Machine learning of nonlinear partial differential equations. *Journal of Computational Physics*, 357, 2018.

Tom Ryder, Andrew Golightly, A. Stephen McGough, and Dennis Prangle. Black-box variational inference for stochastic differential equations. *ICML*. 2018.

Simo Särkkä. *Bayesian Filtering and Smoothing*. Cambridge University Press., 2013.

Simo Särkkä and Juha Sarmavuori. Gaussian filtering and smoothing for continuous-discrete dynamic systems. *Signal Processing*, 93, 2013.

Simo Särkkä and Arno Solin. *Applied Stochastic Differential Equations*. Cambridge University Press., 2019.

Justin A Sirignano and Konstantinos Spiliopoulos. Dgm: A deep learning algorithm for solving partial differential equations. *Journal of Computational Physics*, 375, 2018.

Frank Stenger and John Mcnamee. Construction of fully symmetric numerical integration formulas. *Numerische Mathematik*, 10, 1967.

Belinda Tzen and Maxim Raginsky. Neural stochastic differential equations: Deep latent gaussian models in the diffusion limit. *ArXiv*, abs/1905.09883, 2019.

Eric A. Wan and Rudolph Van Der Merwe. The unscented kalman filter for nonlinear estimation. 2000.

Jack M. Wang, David J. Fleet, and Aaron Hertzmann. Gaussian process dynamical models for human motion. *IEEE Trans. Pattern Anal. Mach. Intell.*, 30, 2008.

Anqi Wu, Sebastian Nowozin, Edward Meeds, Richard E. Turner, Jose Miguel Hernandez-Lobato, and Alexander L. Gaunt. Deterministic variational inference for robust bayesian neural networks. In *ICLR*. 2019.

Shuhuang Xiang and Folkmar Bornemann. On the convergence rates of gauss and clenshaw–curtis quadrature for functions of limited regularity. *SIAM Journal on Numerical Analysis*, 50, 2012.

Cagatay Yildiz, Markus Heinonen, and Harri Lähdesmäki. Ode2vae: Deep generative second order odes with bayesian neural networks. In *NeurIPS*. 2019.

Fisher Yu and Vladlen Koltun. Multi-scale context aggregation by dilated convolutions. In *ICLR*. 2016.

Jiong Zhang, Qi Lei, and Inderjit Dhillon. Stabilizing gradients for deep neural networks via efficient svd parameterization. In *ICML*. 2018.

Tianjun Zhang, Zhewei Yao, Amir Gholami, Joseph E Gonzalez, Kurt Keutzer, Michael W Mahoney, and George Biros. Anodev2: A coupled neural ode framework. In *Neurips*. 2019.

A Proof of Theorem 1 (Marginalizing Stochasticity)

Integrating with respect to \mathbf{w} in order to estimate \mathbf{m}_{k+1} in Eq. 4 can be done directly by applying $\mathbb{E}[\Delta\mathbf{w}] = 0$ together with Euler-Maruyama:

$$\begin{aligned}\mathbf{m}_{k+1} &\triangleq \int \int_{\mathbb{R}^D \times S} \tilde{\mathbf{x}}_{k+1}^{(\theta, \phi)} \underbrace{p_{\theta, \phi}(\mathbf{x}_k, t_k)}_{\approx \mathcal{N}(\mathbf{x}_k | \mathbf{m}_k, \mathbf{P}_k)} p(\mathbf{w}_k) d\mathbf{w}_k d\mathbf{x}_k \\ &= \int \int_{\mathbb{R}^D \times S} [\mathbf{x}_k + \mathbf{f}_\theta(\mathbf{x}_k, t_k) \Delta t + \mathbf{L}_\phi(\mathbf{x}_k, t_k) \Delta \mathbf{w}_k] \mathcal{N}(\mathbf{x}_k | \mathbf{m}_k, \mathbf{P}_k) p(\mathbf{w}_k) d\mathbf{w}_k d\mathbf{x}_k \\ &= \int_{\mathbb{R}^D} \underbrace{[\mathbf{x}_k + \mathbf{f}_\theta(\mathbf{x}_k, t_k) \Delta t]}_{\hat{\mathbf{x}}_{k+1}^{(\theta, \phi)}} \mathcal{N}(\mathbf{x}_k | \mathbf{m}_k, \mathbf{P}_k) d\mathbf{x}_k\end{aligned}$$

For deriving \mathbf{P}_{k+1} using Euler-Maruyama we first rewrite equation 5 as:

$$\begin{aligned}\mathbf{P}_{k+1} &\triangleq \int \int_{\mathbb{R}^D \times S} (\tilde{\mathbf{x}}_{k+1}^{(\theta, \phi)} - \mathbf{m}_{k+1})(\tilde{\mathbf{x}}_{k+1}^{(\theta, \phi)} - \mathbf{m}_{k+1})^T \underbrace{p_{\theta, \phi}(\mathbf{x}_k, t_k)}_{\approx \mathcal{N}(\mathbf{x}_k | \mathbf{m}_k, \mathbf{P}_k)} p(\mathbf{w}_k) d\mathbf{w}_k d\mathbf{x}_k \\ &= \int \int_{\mathbb{R}^D \times S} (\tilde{\mathbf{x}}_{k+1}^{(\theta, \phi)}) (\tilde{\mathbf{x}}_{k+1}^{(\theta, \phi)})^T \mathcal{N}(\mathbf{x}_k | \mathbf{m}_k, \mathbf{P}_k) p(\mathbf{w}_k) d\mathbf{w}_k d\mathbf{x}_k - \mathbf{m}_{k+1} \mathbf{m}_{k+1}^T.\end{aligned}$$

We use the definition of $\tilde{\mathbf{x}}_{k+1}^{(\theta, \phi)} = \mathbf{x}_k + \mathbf{f}_\theta(\mathbf{x}_k, t_k) \Delta t + \mathbf{L}_\phi(\mathbf{x}_k, t_k) \Delta \mathbf{w}_k$ and evaluate the product. For readability we omit the arguments:

$$\begin{aligned}(\tilde{\mathbf{x}}_{k+1}^{(\theta, \phi)}) (\tilde{\mathbf{x}}_{k+1}^{(\theta, \phi)})^T &= (\mathbf{x}_k + \mathbf{f}_\theta \Delta t + \mathbf{L}_\phi \Delta \mathbf{w}_k) (\mathbf{x}_k + \mathbf{f}_\theta \Delta t + \mathbf{L}_\phi \Delta \mathbf{w}_k)^T \\ &= \mathbf{x}_k \mathbf{x}_k^T + \mathbf{x}_k \mathbf{f}_\theta^T \Delta t + \mathbf{x}_k (\mathbf{L}_\phi \Delta \mathbf{w}_k)^T + \mathbf{f}_\theta \Delta t \mathbf{x}_k^T + \mathbf{f}_\theta \mathbf{f}_\theta^T \Delta t^2 + \\ &\quad \mathbf{f}_\theta \Delta t (\mathbf{L}_\phi \Delta \mathbf{w}_k)^T + \mathbf{L}_\phi \Delta \mathbf{w}_k \mathbf{x}_k^T + \mathbf{L}_\phi \Delta \mathbf{w}_k \mathbf{f}_\theta^T \Delta t + \mathbf{L}_\phi \Delta \mathbf{w}_k \Delta \mathbf{w}_k^T \mathbf{L}_\phi^T\end{aligned}$$

We can omit $\Delta \mathbf{w}$ terms as $\mathbb{E}[\Delta \mathbf{w}] = 0$, as well as $\Delta \mathbf{w} \Delta t$ and $\Delta \mathbf{w}$, since $\mathbb{E}[\Delta \mathbf{w} \Delta t] = \mathbb{E}[\Delta \mathbf{w}] \mathbb{E}[\Delta t] = 0$. The outer product $\Delta \mathbf{w}_k \Delta \mathbf{w}_k^T$ results in a symmetric matrix with shape $\mathbb{R}^{S \times S}$. From Itô calculus [Oksendal, 1992] $\mathbb{E}[\Delta \mathbf{w}_{k,i}^2] = \Delta t$ follows. This equality only applies to the diagonal entries of resulting matrix $\Delta \mathbf{w}_k \Delta \mathbf{w}_k^T$, offdiagonal values may be omitted, since $\mathbb{E}[\Delta \mathbf{w}_{k,i} \Delta \mathbf{w}_{k,j}] = \mathbb{E}[\Delta \mathbf{w}_{k,i}] \mathbb{E}[\Delta \mathbf{w}_{k,j}] = 0$. We thus can write the solution to the integral with respect to $p(\Delta \mathbf{w}_k)$ in a closed form:

$$\mathbb{E}_{\Delta \mathbf{w}_k} [(\tilde{\mathbf{x}}_{k+1}^{(\theta, \phi)}) (\tilde{\mathbf{x}}_{k+1}^{(\theta, \phi)})^T] = \underbrace{(\mathbf{x}_k + \mathbf{f}_\theta \Delta t) (\mathbf{x}_k + \mathbf{f}_\theta \Delta t)^T + \mathbf{L}_\phi \mathbf{L}_\phi^T \Delta t}_{\hat{\mathbf{x}}_{k+1}^{(\theta, \phi)}}.$$

Finally we arrive at a tractable form of the integral:

$$\begin{aligned}\mathbf{P}_{k+1} &= \int \int_{\mathbb{R}^D \times S} (\tilde{\mathbf{x}}_{k+1}^{(\theta, \phi)}) (\tilde{\mathbf{x}}_{k+1}^{(\theta, \phi)})^T \mathcal{N}(\mathbf{x}_k | \mathbf{m}_k, \mathbf{P}_k) p(\mathbf{w}_k) d\mathbf{w}_k d\mathbf{x}_k - \mathbf{m}_{k+1} \mathbf{m}_{k+1}^T \\ &= \int_{\mathbb{R}^D} \left[(\hat{\mathbf{x}}_{k+1}^{(\theta, \phi)}) (\hat{\mathbf{x}}_{k+1}^{(\theta, \phi)})^T + \mathbf{L}_\phi \mathbf{L}_\phi^T \Delta t \right] \mathcal{N}(\mathbf{x}_k | \mathbf{m}_k, \mathbf{P}_k) d\mathbf{x}_k - \mathbf{m}_{k+1} \mathbf{m}_{k+1}^T \\ &= \int_{\mathbb{R}^D} \left[(\hat{\mathbf{x}}_{k+1}^{(\theta, \phi)} - \mathbf{m}_{k+1}) (\hat{\mathbf{x}}_{k+1}^{(\theta, \phi)} - \mathbf{m}_{k+1})^T + \mathbf{L}_\phi \mathbf{L}_\phi^T (\mathbf{x}_k, t_k) \Delta t \right] \mathcal{N}(\mathbf{x}_k | \mathbf{m}_k, \mathbf{P}_k) d\mathbf{x}_k,\end{aligned}$$

which can be solved with a numerical cubature integration method.

B Proof of Theorem 2 (Covariance Stability)

Proof by induction.

Proposition. \mathbf{P}_k is PSD if \mathbf{P}_1 is PSD, $\forall k \in \mathbb{N}$.

Base Case. If $k = 1$, \mathbf{P}_1 is PSD by initial proposition. If $k = 2$, \mathbf{P}_2 is estimated by:

$$\begin{aligned}\mathbf{P}_2 &= \int_{\mathbb{R}^D} \underbrace{\left[(\hat{\mathbf{x}}_2^{(\theta, \phi)} - \mathbf{m}_2) (\hat{\mathbf{x}}_2^{(\theta, \phi)} - \mathbf{m}_2)^T + \mathbf{L}_\phi \mathbf{L}_\phi^T (\mathbf{x}_1, t_1) \Delta t \right]}_{\mathbf{g}(\cdot)} \mathcal{N}(\mathbf{x}_1 | \mathbf{m}_1, \mathbf{P}_1) d\mathbf{x}_1 \\ &\approx \sum_{i=1}^C w_i \mathbf{g}(\mathbf{m}_1 + \sqrt{\mathbf{P}_1} \zeta_i, t_1)\end{aligned}$$

Since \mathbf{P}_1 is PSD, it is possible to calculate $\sqrt{\mathbf{P}_1}$. The covariance \mathbf{P}_2 is estimated via QMC, which amounts to a weighted sum. Each summand $\mathbf{g}(\cdot)$ is a sum positive semi-definite matrices. A sum of PSD matrices is again PSD. Let \mathbf{A} be such a sum of N PSD matrices \mathbf{A}_i :

$$\mathbf{x}^T \left(\sum_i \mathbf{A}_i \right) \mathbf{x} = \sum_i \underbrace{\mathbf{x}^T \mathbf{A}_i \mathbf{x}}_{\geq 0} \geq 0,$$

hence \mathbf{A} is PSD. We conclude that \mathbf{P}_2 is PSD independent of step size Δt .

Inductive Step. The covariance of \mathbf{P}_{k+1} is depending on \mathbf{P}_k . Since \mathbf{P}_k is PSD, \mathbf{P}_{k+1} must be also PSD following the reasoning of the base case. We conclude that \mathbf{P}_k is PSD if \mathbf{P}_1 is PSD, $\forall k \in \mathbb{N}$.

C Proof of Theorem 3 (Weak Convergence)

Definition 2 (linear growth). $\mathbf{f}_\theta(\mathbf{x}, t)$ and $\mathbf{L}_\phi(\mathbf{x}, t)$ are at most linear if:

$$|\mathbf{f}_\theta(\mathbf{x}, t)| + |\mathbf{L}_\phi(\mathbf{x}, t)| \leq c_1(1 + |\mathbf{x}|), \quad \exists c_1 > 0, \forall \mathbf{x} \in \mathbb{R}^D, \forall t \in \mathbb{R}^+.$$

Definition 3 (c_2 -Lipschitz). $\mathbf{f}_\theta(\mathbf{x}, t)$ and $\mathbf{L}_\phi(\mathbf{x}, t)$ are c_2 -Lipschitz if:

$$|\mathbf{f}_\theta(\mathbf{x}, t) - \mathbf{f}_\theta(\mathbf{y}, t)| + |\mathbf{L}_\phi(\mathbf{x}, t) - \mathbf{L}_\phi(\mathbf{y}, t)| \leq c_2(|\mathbf{x} - \mathbf{y}|), \quad \exists c_2 > 0, \forall \mathbf{x}, \mathbf{y} \in \mathbb{R}^D, \forall t \in \mathbb{R}^+.$$

Proof. Weak convergence of our method DI-NSDE can be derived directly from EM convergence. We start from our algorithm and recover the original definition of the weak convergence proof of the EM discretization. Expectation $\mathbb{E}[\cdot]$ is calculated with respect to \mathbf{w} and \mathbf{x} . After integrating analytically with respect to \mathbf{w} the smooth function $\mathbf{g}(\cdot)$ is changed to $\mathbf{g}_\mathbf{w}(\cdot)$.

$$\begin{aligned} \lim_{C \rightarrow +\infty} \sup_{0 \leq t_k \leq T} \left| \mathbb{E}[\mathbf{g}(\mathbf{x}_k)] - \sum_{i=1}^C w_i \mathbf{g}_\mathbf{w}(\mathbf{m}_k + \sqrt{\mathbf{P}_k} \zeta_i, t_k) \right| &= \text{QMC-Error} \rightarrow 0 \\ \sup_{0 \leq t_k \leq T} \left| \mathbb{E}[\mathbf{g}(\mathbf{x}_k)] - \mathbb{E}_{\tilde{\mathbf{x}}_k \sim \mathcal{N}}[\mathbf{g}_\mathbf{w}(\tilde{\mathbf{x}}_k)] \right| &= p(\mathbf{x}_k), p(\tilde{\mathbf{x}}_k) \text{ are Gaussian} \\ \sup_{0 \leq t_k \leq T} \left| \mathbb{E}[\mathbf{g}(\mathbf{x}_k)] - \mathbb{E}_{\tilde{\mathbf{x}}_k \sim p(\tilde{\mathbf{x}}_k)}[\mathbf{g}_\mathbf{w}(\tilde{\mathbf{x}}_k)] \right| &= \text{Analytical Integral } \mathbf{w} \\ \sup_{0 \leq t_k \leq T} \left| \mathbb{E}[\mathbf{g}(\mathbf{x}_k)] - \mathbb{E}_{\substack{\mathbf{w} \sim p(\mathbf{w}) \\ \tilde{\mathbf{x}}_k \sim p(\tilde{\mathbf{x}}_k)}}[\mathbf{g}(\tilde{\mathbf{x}}_k)] \right| &\leq S \Delta t, \quad \exists S \in \mathbb{R}^+. \quad \text{Weak-Convergence} \end{aligned}$$

Convergence of QMC is at least $\mathcal{O}(C^{-\alpha})$, with C being the number of particles and $\alpha \geq 1$ a task specific constant [Xiang and Bornemann, 2012]. Linear growth and c_2 -Lipschitz condition of $\mathbf{f}_\theta(\mathbf{x}), \mathbf{L}_\phi(\mathbf{x})$ are necessary conditions of the weak convergence proof [Kloeden and Platen, 2013]. In general this assumption is valid for neural networks, when the activation functions follow these conditions.

D ODE-Based Approximations of Mean and Covariance

Firstly we sketch the derivation of the ODEs for mean $\frac{\partial \mathbf{m}}{\partial t} = \dot{\mathbf{m}}$ and covariance $\frac{\partial \mathbf{P}}{\partial t} = \dot{\mathbf{P}}$ evolution when dynamics is governed by an SDE (ODE approximation, ODEA). Therefor we review the infinitesimal generator (think of it for simplicity as the time derivative $\frac{\partial}{\partial t}$) of some general function g as the operator \mathcal{A} [Oksendal, 1992]:

$$\mathcal{A}g = \frac{\partial g}{\partial t} + \nabla_{\mathbf{x}} g \mathbf{f}(\mathbf{x}, t) + \frac{1}{2} \sum_{i,j} \frac{\partial^2 g}{\partial x_i \partial x_j} [\mathbf{L} \mathbf{L}^T(\mathbf{x}, t)]_{i,j}.$$

Taking the expected value and using the function $g = x_i$, with the i -th component of \mathbf{x} , we obtain after vectorizing, the time evolution of the mean as:

$$\frac{d\mathbf{m}}{dt} = \mathbb{E}[\mathbf{f}(\mathbf{x}, t)]. \quad (12)$$

In a similar way we obtain the time evolution of the covariance by taking the expected value, using the function $g = x_i x_j - m_i m_j$, and vectorizing:

$$\frac{d\mathbf{P}}{dt} = \mathbb{E}[\mathbf{f}(\mathbf{x}, t)(\mathbf{x} - \mathbf{m})^T] + \mathbb{E}[(\mathbf{x} - \mathbf{m})\mathbf{f}^T(\mathbf{x}, t)] + \mathbb{E}[\mathbf{L} \mathbf{L}^T(\mathbf{x}, t)]. \quad (13)$$

Note that these ODEs are usually not solvable, since the expectation is calculated with respect to the potentially complicated distribution $p(\mathbf{x}, t)$. Throughout the paper we use the approximation $p(\mathbf{x}, t) \approx \mathcal{N}(\mathbf{x} | \mathbf{m}(t), \mathbf{P}(t))$. In order to obtain the desired result at time T , one needs to choose a suitable ODE-Solver, such as Runge-Kutta, and integrate up to time T . Often it is assumed that the starting distribution at time $t = 0$ is Dirac delta distributed, which can be approximated by a Gaussian with small covariance, i.e. $\mathbf{P} \approx \mathbf{I}\epsilon$, with \mathbf{I} representing the identity matrix and a small $\epsilon > 0$.

Cubature approximation. Using a cubature method (here unscented transform UT) together with the two ODEs for mean and covariance (Eq. 12 and 13) we obtain the tractable approximation:

$$\begin{aligned}\frac{d\mathbf{m}}{dt} &= \sum_{i=0}^{2D} w_i \mathbf{f}(\mathbf{m} + \sqrt{\mathbf{P}} \boldsymbol{\zeta}_i, t) \\ \frac{d\mathbf{P}}{dt} &= \sum_{i=0}^{2D} w_i \left[\mathbf{f}(\mathbf{m} + \sqrt{\mathbf{P}} \boldsymbol{\zeta}_i, t) \boldsymbol{\zeta}_i^T \sqrt{\mathbf{P}}^T + \sqrt{\mathbf{P}} \boldsymbol{\zeta}_i \mathbf{f}(\mathbf{m} + \sqrt{\mathbf{P}} \boldsymbol{\zeta}_i, t)^T + \mathbf{L} \mathbf{L}^T (\mathbf{m} + \sqrt{\mathbf{P}} \boldsymbol{\zeta}_i, t) \right].\end{aligned}$$

We refer to this approximation to as ODE approximation via unscented transform (ODEA_{UT}).

Linearized approximation. The linearized approximation builds on a Taylor expansion of the governing SDE. Thus the drift and diffusion of the SDE is linearized as [Särkkä and Solin, 2019]:

$$\begin{aligned}\mathbf{f}(\mathbf{x}, t) &\approx \mathbf{f}(\mathbf{m}, t) + \mathbf{F}_x(\mathbf{m}, t)(\mathbf{x} - \mathbf{m}) \\ \mathbf{L}(\mathbf{x}, t) &\approx \mathbf{L}(\mathbf{m}, t),\end{aligned}$$

with the Jacobian $\mathbf{F}_x(\mathbf{x}) = \frac{\partial \mathbf{f}(\mathbf{x})}{\partial \mathbf{x}}$. Note that we approximated the drift as a constant in order to keep computational overhead feasible. For covariance approximation, we also use the equality [Särkkä and Sarmavuori, 2013]

$$\mathbb{E}[\mathbf{f}(\mathbf{x}, t)(\mathbf{x} - \mathbf{m})] = \mathbb{E}[\mathbf{F}_x(\mathbf{x}, t)] \mathbf{P},$$

where $\mathbf{x} \sim \mathcal{N}(\mathbf{m}, \mathbf{P})$. Using these two equations together with the original ODEs (Eq. 12 and 13) we obtain:

$$\begin{aligned}\frac{d\mathbf{m}}{dt} &= \mathbf{f}(\mathbf{m}, t) \\ \frac{d\mathbf{P}}{dt} &= \mathbf{P} \mathbf{F}_x(\mathbf{m}, t)^T + \mathbf{F}_x(\mathbf{m}, t) \mathbf{P}^T + \mathbf{L} \mathbf{L}^T (\mathbf{m}, t).\end{aligned}$$

We refer to this method as ODE approximation via linearization (ODEA_{Lin.}), which found widespread use in the context of extended Kalman filters [Brown and Hwang, 1997]. The present auto-diff libraries provide methods for calculating the Jacobian, though not efficiently off-the-shelf, since they are optimized for Vector-Jacobian products. For the linear case, this approximation is fully correct. Hence, we can recover the solution proposed in [Archambeau et al., 2007] when using only affine transformations for $\mathbf{L}(\mathbf{x}, t)$ and $\mathbf{f}(\mathbf{x}, t)$.

E Covariance Stability of ODEA Alternatives

In this section we discuss covariance stability (Definition 1) of the alternative methods ODEA_{UT/Lin.}.

ODEA_{Lin.}. First lets review the time derivative of \mathbf{P} . By inspecting each summand separately it is obvious, that \mathbf{P}_k will not be estimated as a sum PSD matrices (independent of chosen numerical solver). Hence after several solver steps, accumulating numerical errors can result in an ill defined \mathbf{P}_k . However the time derivative of \mathbf{P} resembles the differential Riccati equation (DRE). A DRE is usually stiff and demands in turn implicit solvers in order to ensure well-defined results. We refer to Mena and Benner [2007] for a detailed discussion on numerical solution methods for a DRE. We further denote, that such implicit solvers are not readily available for NSDEs [Chen et al., 2018, Li et al., 2020] and offer an interesting future direction.

$$\frac{d\mathbf{P}}{dt} = \underbrace{\mathbf{P} \mathbf{F}_x(\mathbf{m}, t)^T + \mathbf{F}_x(\mathbf{m}, t) \mathbf{P}^T}_{\text{Symmetric} \neq \text{PSD}} + \underbrace{\mathbf{L} \mathbf{L}^T(\mathbf{m}, t)}_{\text{PSD}}$$

Differential Riccati Equation $\rightarrow \dot{\mathbf{P}} = \mathbf{P} \mathbf{A} + \mathbf{A}^T \mathbf{P} + \mathbf{Q}$

ODEA_{UT}. With the same reasoning as before, we first review each summand of the time derivative. Again we can tell by inspection, that \mathbf{P}_k will not be estimated as a sum PSD matrices (independent of chosen numerical solver). Hence after several solver steps, accumulating numerical errors can result in an ill defined \mathbf{P}_k . Unfortunately the $\dot{\mathbf{P}}$ does not resemble the well studied DRE this time, though having similar structure. Hence theoretical guarantees are not known to exist even for implicit solvers.

$$\begin{aligned}\frac{d\mathbf{P}}{dt} &= \sum_{i=0}^{2D} w_i \left[\underbrace{\mathbf{f}(\mathbf{m} + \sqrt{\mathbf{P}} \boldsymbol{\zeta}_i, t) \boldsymbol{\zeta}_i^T \sqrt{\mathbf{P}}^T + \sqrt{\mathbf{P}} \boldsymbol{\zeta}_i \mathbf{f}(\mathbf{m} + \sqrt{\mathbf{P}} \boldsymbol{\zeta}_i, t)^T}_{\text{Symmetric} \neq \text{PSD}} + \underbrace{\mathbf{L} \mathbf{L}^T(\mathbf{m} + \sqrt{\mathbf{P}} \boldsymbol{\zeta}_i, t)}_{\text{PSD}} \right] \\ &= \underbrace{\left[\sum_{i=0}^{2D} w_i \mathbf{f}(\boldsymbol{\chi}_i, t) \boldsymbol{\zeta}_i^T \right]}_{\mathbf{A}^T} \sqrt{\mathbf{P}}^T + \sqrt{\mathbf{P}} \underbrace{\left[\sum_{i=0}^{2D} w_i \boldsymbol{\zeta}_i \mathbf{f}(\boldsymbol{\chi}_i, t)^T \right]}_{\mathbf{A}} + \underbrace{\sum_{i=0}^{2D} w_i \mathbf{L} \mathbf{L}^T(\boldsymbol{\chi}_i, t)}_{\mathbf{Q}} \\ &= \mathbf{A}^T \sqrt{\mathbf{P}}^T + \sqrt{\mathbf{P}} \mathbf{A} + \mathbf{Q}\end{aligned}$$

F Log-Likelihood via Cholesky Decomposed

Suppose you want to calculate the log-likelihood for a multivariate Gaussian:

$$p(\mathbf{x}_{k+1}|\mathbf{x}_k) = \mathcal{N}(\mathbf{x}_{k+1}|\mathbf{m}_{k+1}, \mathbf{P}_{k+1}) = \frac{\exp\left(-\frac{1}{2}d(\mathbf{x}_{k+1}, \mathbf{m}_{k+1}, \mathbf{P}_{k+1})^2\right)}{\sqrt{(2\pi)^D |\mathbf{P}_{k+1}|}}$$

, where $d(\mathbf{x}_{k+1}, \mathbf{m}_{k+1}, \mathbf{P}_{k+1})$ is the Mahalanobis distance. Since it is required to compute the inverse and determinant of \mathbf{P}_{k+1} , it is beneficial to calculate its Cholesky decomposed $\sqrt{\mathbf{P}_{k+1}}$ and use it for calculation of both target quantities. Thus the two identities, which apply for any positive semi-definite matrix \mathbf{P} , can be used:

$$|\mathbf{P}| = |\sqrt{\mathbf{P}}|^2 = \left(\prod_{i=1}^D \sqrt{\mathbf{P}_{i,i}} \right)^2$$

$$\mathbf{P}^{-1} = \left(\sqrt{\mathbf{P}}^{-1} \right) \left(\sqrt{\mathbf{P}}^{-1} \right)^T$$

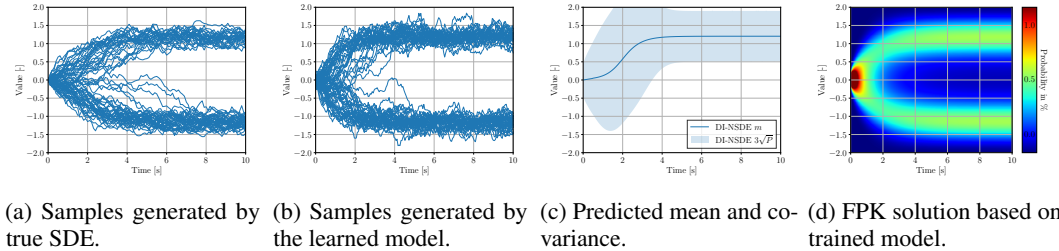
The inverse Cholesky decomposed can be fastly calculated by solving a linear system of equations.

G Fitting Multimodal Processes

This section explores certain theoretical properties and limitations of our method on synthetic multimodal data. We generate the true data distribution by following one-dimensional SDE:

$$dx = \tanh(x)(\mu - \tanh(x)x)dt + 2dw,$$

with $\mu = 1$. For training purposes, we generate 128 sequences with $t \in [0, 10]$ s and $\Delta t = 0.1$ s. Fig. 4a shows the true data distribution and Fig. 4b the generated samples by using Euler-Maruyama discretization after training a model using DI-NSDE. The generated samples match the multimodality of the true distribution, though the model was trained using an assumed Gaussian transition probability. During training we used shorter and randomly picked snippets (10 time steps) for which the Gaussian assumption is valid. Thus the final model covers both modes.



(a) Samples generated by true SDE. (b) Samples generated by the learned model. (c) Predicted mean and covariance. (d) FPK solution based on trained model.

Figure 4: Dynamics of true SDE and trained neural SDE with DI-NSDE on a synthetic multimodal data distribution.

However, when making long-term predictions (100 steps) using DI-NSDE one can see in Fig. 4c, that the prediction sticks to one of the two modes. When using different starting points for long-term predictions, it is hardly possible to determine which of the two modes will be picked. Thus, using DI-NSDE in downstream tasks together with an underlying multimodal data distribution may cause instabilities or unforeseeable predictions. We also evaluate the learned model by solving the underlying FPK equation. We use the finite-difference method with a grid size of $\Delta x = 10^{-2}$ and a time step of $\Delta t = 10^{-4}$ s. A Dirichlet boundary condition is used, ensuring that $p(x = -2) = p(x = 2) = 0$. Indeed one can see in Fig. 4d that the model recovers the true data distribution. Thus, DI-NSDE may also be used for training a NSDE on a multimodal data distribution, since the Gaussian assumption is usually valid for shorter snippets. However special care needs to be taken for long-term predictions, by e.g. comparing the sampled distribution with predicted distribution via DI-NSDE.

H Numerical Error of quasi Monte-Carlo Integration

We investigate the accuracy of the QMC approximation depending on dimensionality and function complexity. We initialize a random Gaussian distribution with diagonal covariance and pass it through a random neural network with defined dimensionality (input and output having same number of dimensions) and function complexity (number of layers). We estimate the mean and covariance of the output distribution by passing 10^6 samples through the network. This distribution is denoted as the ground truth P_{True} . Using the same random initialized network and distribution we estimate the output distribution using a QMC approximation,

i.e. unscented transform. Additionally we estimate the output distribution using layerwise moment matching. Layerwise moment matching is also able to calculate in a deterministic way the output distribution, when using smooth and monotonic activation functions [Wu et al., 2019]. We use here $\tanh(\cdot)$ as the activation function and estimate the output approximated by layerwise moment matching by sampling using 10^6 samples. We repeat each experiment for each configuration 32 times and estimate the Kullback-Leibler divergence between the two approximations and the true distribution. Error of UT is not depending on function complexity and increases for higher dimensionality. Layerwise moment matching results in high error if more than one layer is used. This may change when Bayesian networks are used since off diagonal values entries in the covariance matrix may be reduced compared to diagonal ones and the error by applying central limit theorem may decrease. As a result UT is applicable especially for lower dimensionality.

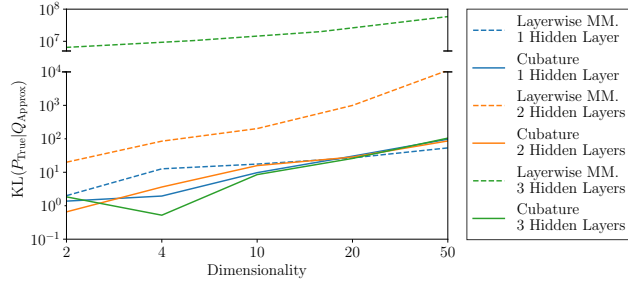
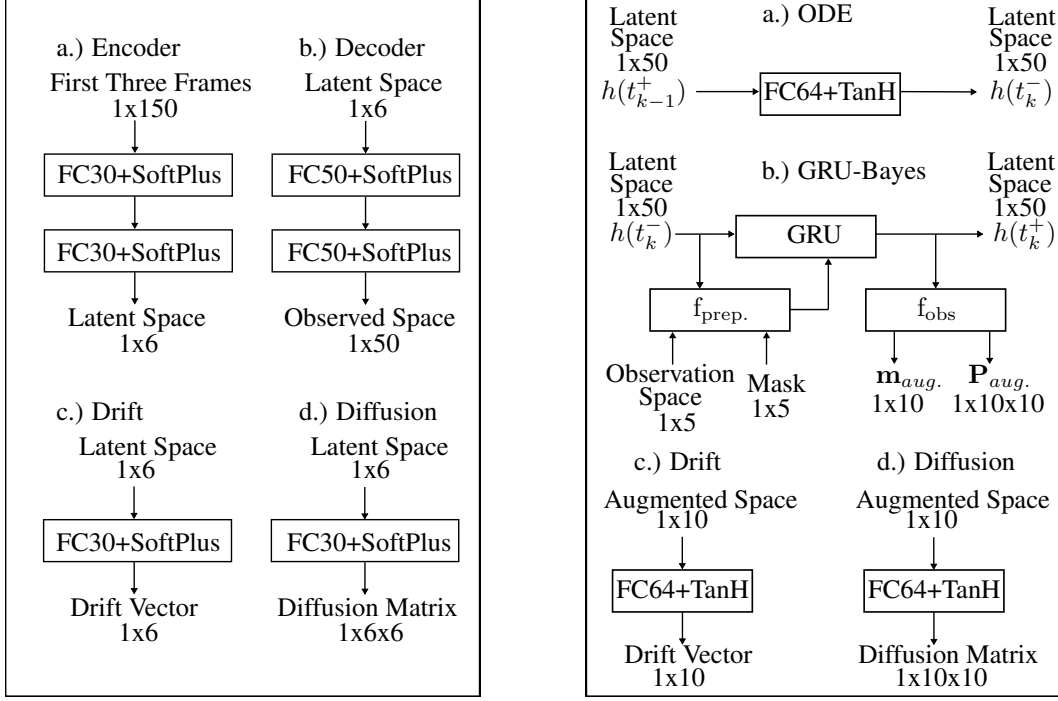


Figure 5: KL-divergence between true resulting distribution and different approximation techniques (layerwise moment matching [Wu et al., 2019] and cubature method) depending on dimensionality and number of hidden layers. We pass for each configuration 32 random Gaussian distributions with diagonal covariance through a random initialized neural network. The true distribution is estimated by sampling, using 10^6 draws. For calculation of KL-divergence first two moments are used.

I Stochastic Lotka-Volterra Equation

We choose the true dynamics of stochastic Lotka-Volterra equations as in [Abbat et al., 2019]:

$$d\mathbf{x} = \begin{bmatrix} 2x_1 - x_1 x_2 \\ x_1 x_2 - 4x_2 \end{bmatrix} dt + \sqrt{\begin{bmatrix} 0.05 & 0.03 \\ 0.03 & 0.09 \end{bmatrix}} d\mathbf{w}.$$



(a) Architecture used for CMU walking data. Our model has similar number of parameters (11.9k) compared to current state of the art model [Yildiz et al., 2019] (12.1k).

(b) Architecture used for USHCN weather prediction task. We adapt the architecture from Brouwer et al. [2019] for encoding a sequence of partially observed data points. Our model has 40.5k parameters compared to current state of the art model [Brouwer et al., 2019] with 24.7k parameters.

Figure 6: Sketches of model architectures.

J Model Architectures

In this chapter we describe the model architectures used in the real world experiments.

J.1 CMU Walking Data

For the CMU walking experiment we use the same encoder-decoder structure as in [Yildiz et al., 2019]. The encoder takes the first three frames and maps it to a latent space. In the latent space we define a SDE in order to estimate mean and covariance at each time step. At every time step we take the predicted mean and covariance and pass it through the decoder network. We estimate mean and covariance of the decoder with unscented transform. Thus the model is also directly runnable in sampling mode without any modifications.

J.2 Climate Forecast

An encoder-decoder structure is used in the climate forecasting experiment. The encoder is a simplified GRU-ODE-Bayes model [Brouwer et al., 2019], which consists of the ODE model and GRU-Bayes model. The ODE model is used to model the dynamics between observations. It takes the previous latent variable $\mathbf{h}(t_{k-1}^+)$ as the input and outputs $\mathbf{h}(t_k^-)$ as the predicted latent variable at the current time point. The GRU-Bayes model is used to update the latent variable from $\mathbf{h}(t_k^-)$ to $\mathbf{h}(t_k^+)$, if there is an observation. Due to missed values, the partially-observed vector needs to be preprocessed before going into the GRU unit. The update and preprocessing are the same as in [Brouwer et al., 2019]. Conditioned on $\mathbf{h}(t_k^+)$, the observation model can predict the mean \mathbf{m}_k and covariance \mathbf{P}_k in the augmented space. We use DI-NSDE for the decoder, which works in the augmented space [Dupont et al., 2019]. It takes the last outputs of the encoder as the initial mean and covariance and does predictions recursively. The first 5 dimensions of the SDE are outputted as the prediction. Our loss function is the negative log-likelihood of a multivariate Gaussian distribution. Since the data is only sporadically observed, we need to marginalize out the unobserved dimensions.

K Further Climate Predictions

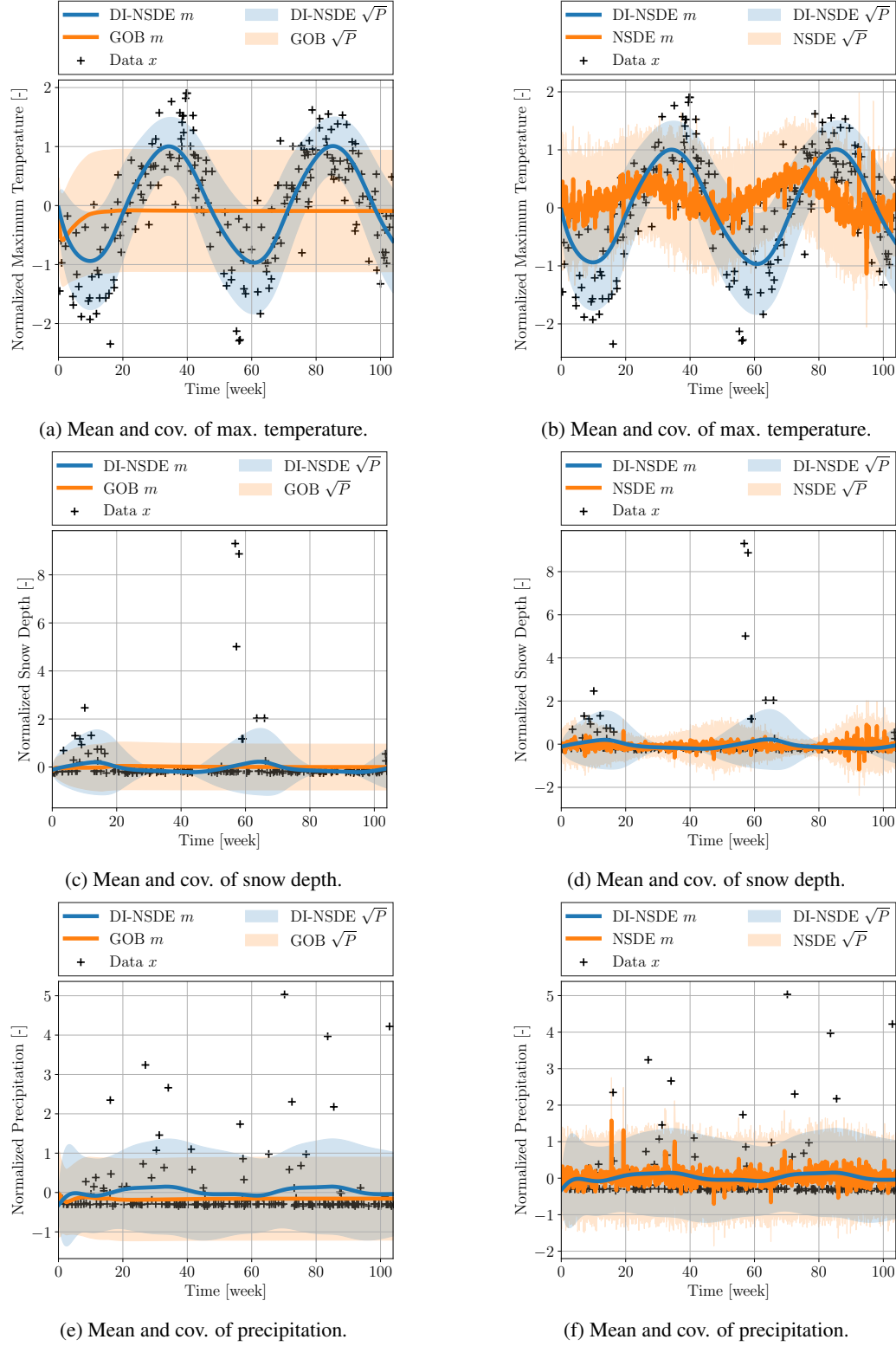


Figure 7: DI-NSDE_{Lin.}, NSDE_{MC}, and GOB [Brouwer et al., 2019] predictions for USHCN daily dataset.

L Python Code

```

55     P_next = P_next.view(bs, n_pts, dim, dim)
56     P_next = torch.sum(P_next, 1)
57
58     t_next = t + dt
59
60     return m_next, P_next, t_next
61
62 def integrate(function, m, P):
63     """Estimates of mean m and covariance P of the output when a Gaussian variable is ↴
64     passed through a function f.
65
66     Args:
67         f (nn.Module): Module implementation in PyTorch. Standard implementation, takes ↴
68             input x and outputs x_out
69         m (Tensor): mean
70         P (Tensor): covariance
71
72     Returns:
73         m_out (Tensor): mean of function output
74         P_out(Tensor): covariance of function output
75     """
76
77     bs, dim = m.shape
78     n_pts = 2*dim + 1
79
80     z, w = unscented_pts(dim)
81     z = torch.FloatTensor(z).view(n_pts, dim, 1)
82     w = torch.FloatTensor(w).view(n_pts, 1)
83
84     # Get next batch of mean values by cubature
85     m_rep = torch.repeat_interleave(m, repeats=n_pts, dim=0)
86     P_chol = torch.cholesky(P)
87     P_chol_rep = torch.repeat_interleave(P_chol, repeats=n_pts, dim=0)
88
89     z_rep = z.repeat(bs, 1, 1)
90     w_rep = w.repeat(bs, 1)
91
92     # gives you cubature points
93     inputs = m_rep + (P_chol_rep @ z_rep).squeeze()
94     # pass through func
95     outs = function(inputs)
96     # sum up and get mean
97     m_out = outs * w_rep
98     m_out = torch.sum(m_out.view(bs, n_pts, -1), 1)
99
100    # reuse function call for covariance
101    m_out_rep = torch.repeat_interleave(m_out, repeats=n_pts, dim=0)
102
103    # get integral [f(x)-mean] [f(x)-mean]^T dx
104    P_out = (outs - m_out_rep).unsqueeze(-1)
105    P_out = P_out @ P_out.transpose(1, 2)
106    P_out = P_out * w_rep.unsqueeze(-1)
107    d_out = P_out.shape[1] # output dim
108    P_out = P_out.view(bs, n_pts, d_out, d_out)
109    P_out = torch.sum(P_out, 1)
110
111    return m_out, P_out

```